STRUCTURAL BIOLOGY COMMUNICATIONS

ISSN 2053-230X

Structure of the outer membrane porin OmpW from the pervasive pathogen *Klebsiella pneumoniae*

Chloe Seddon,[a,b] Gad Frankel[a] and Konstantinos Beis[a,b]*

[a]Department of Life Sciences, Imperial College, London, United Kingdom, and [b]Rutherford Appleton Laboratory, Research Complex at Harwell, Didcot OX11 0FA, United Kingdom. *Correspondence e-mail: kbeis@imperial.ac.uk

Received 1 November 2023
Accepted 11 December 2023

Edited by G. G. Privé, University of Toronto, Canada

Keywords: *Klebsiella pneumoniae*; outer membrane porin; OmpW; bacterial conjugation; β-barrel.

PDB reference: OmpW from *Klebsiella pneumoniae*, 8qxp

Supporting information: this article has supporting information at journals.iucr.org/f

Conjugation is the process by which plasmids, including those that carry antibiotic-resistance genes, are mobilized from one bacterium (the donor) to another (the recipient). The conjugation efficiency of IncF-like plasmids relies on the formation of mating-pair stabilization via intimate interactions between outer membrane proteins on the donor (a plasmid-encoded TraN isoform) and recipient bacteria. Conjugation of the R100-1 plasmid into *Escherichia coli* and *Klebsiella pneumoniae* (KP) recipients relies on pairing between the plasmid-encoded TraNα in the donor and OmpW in the recipient. Here, the crystal structure of *K. pneumoniae* OmpW ($OmpW_{KP}$) is reported at 3.2 Å resolution. $OmpW_{KP}$ forms an eight-stranded β-barrel flanked by extracellular loops. The structures of *E. coli* OmpW ($OmpW_{EC}$) and $OmpW_{KP}$ show high conservation despite sequence variability in the extracellular loops.

1. Introduction

Outer membrane porins (OMPs) are an important class of β-barrel proteins that form water-filled channels in Gram-negative bacteria. They enable the diffusion of nutrients and the efflux of toxins across the outer membrane (Lou *et al.*, 2009). From a clinical perspective, OMPs are important in modulating the diffusion of antibiotics into the bacterial cell, where mutations or reduced expression of the OMPs enhance antibiotic resistance (Pagès *et al.*, 2008). It has also been shown that OMPs participate in F-like plasmid conjugation, a form of horizontal gene transfer where plasmids are transferred from donor to recipient bacteria in a contact-dependent manner (Lederberg & Tatum, 1946; Frankel *et al.*, 2023). We have recently shown that the efficient conjugation of the multidrug-resistant R100-1 plasmid into both *Escherichia coli* (EC) and *Klebsiella pneumoniae* (KP) relies on the formation of mating-pair stabilization via interaction between the R100-1-encoded OM protein TraNα in the donor and the OMP $OmpW_{EC}$ or $OmpW_{KP}$ in the recipient (Low *et al.*, 2022, 2023). Pairing of the TraN isoform with recipient receptors mediates conjugation species specificity and host range; an in-depth review of mating-pair stabilization and the role of TraN has been provided by Frankel *et al.* (2023). In brief, TraN is an outer membrane protein that is composed of two domains, a base and an extended tip; the base consists of a conserved amphipathic α-helix that possibly anchors TraN to the OM, whereas the tip is mostly comprised of β-sheets linked to a β-sandwich domain. The loops at the tip function as a TraN sensor that participates in recipient selection (Frankel *et al.*, 2023)

In addition to its role in conjugation, OmpW contributes to virulence as the upregulation of $OmpW_{EC}$ increases resistance to host immune defence (Wu *et al.*, 2013). Conversely, OmpW is a key antigen; indeed, OmpW-immunized mice show greater protection against bacterial infections. This could pave the

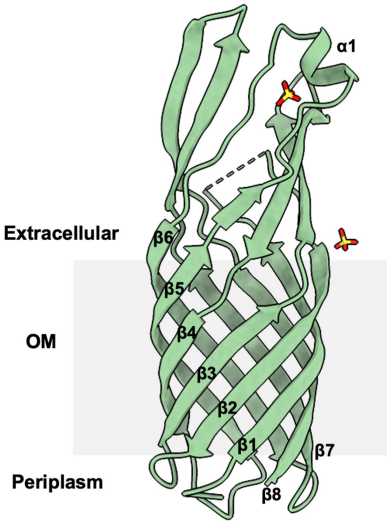

way for the use of OmpW in vaccine preparation (Huang *et al.*, 2015).

The crystal structure of $OmpW_{EC}$ forms an eight-stranded monomeric β-barrel with an extracellular region that is involved in hydrophobic substrate binding (Hong *et al.*, 2006). Here, we present the crystal structure of $OmpW_{KP}$ at 3.2 Å resolution and draw structural comparisons with $OmpW_{EC}$, both of which are conjugation receptors for TraNα.

2. Materials and methods

2.1. Macromolecule production

The mature protein sequence of $OmpW_{KP}$ (His22–Phe212) was subcloned into the pTAMANHISTEV vector in-frame with a *tamA* signal sequence followed by an N-terminal His_7 tag and a Tobacco etch virus (TEV) cleavage site, using the NcoI and XhoI restriction-enzyme sites. The construct was transformed into *E. coli* BL21 C43(DE3) competent cells [F^- *ompT* hsd_{SB} (r_B^- m_B^-) *gal dcm* (DE3)] (Miroux & Walker, 1996) and expressed in Terrific Broth (TB) medium. Cultures were incubated at 37°C with orbital shaking at 200 rev min^{-1} until an optical density at 600 nm (OD_{600}) of 0.6–0.8 was achieved. Cultures were then induced with isopropyl β-D-1-thiogalactopyranoside (IPTG) at a final concentration of 1 m*M* and maintained for 3 h. The cells were harvested by centrifugation (Beckman Coulter) at 8000*g* for 10 min and stored at −80°C. Outer membranes were prepared as described previously (Beis *et al.*, 2006) and were then solubilized in phosphate-buffered saline (PBS) supplemented with 1% *N*,*N*-dimethyl-*n*-dodecylamine *N*-oxide (LDAO) overnight. Unsolubilized membranes and debris were removed by ultracentrifugation at 131 000*g* for 1 h. The supernatant was supplemented with 30 m*M* imidazole and passed through a 5 ml HisTrap HP column (Cytiva) equilibrated in PBS with 0.1% LDAO. The column was washed with 20 column volumes of buffer consisting of PBS, 300 m*M* NaCl, 30 m*M* imidazole pH 7.0 and 0.45% 1-*O*-(*n*-octyl)-tetraethyleneglycol (C_8E_4) to exchange the detergent. $OmpW_{KP}$ was eluted in buffer consisting of 250 m*M* imidazole and 0.45% C_8E_4. $OmpW_{KP}$ was then exchanged into 50 m*M* NaCl, 10 m*M* HEPES pH 7.0 and 0.45% C_8E_4 using a PD-10 Desalting Column (Cytiva) and concentrated to 15 mg ml^{-1}. Macromolecule-production information is summarized in Table 1.

Table 1
$OmpW_{KP}$ construct design.

Source organism	*Klebsiella pneumoniae*
DNA source	*K. pneumoniae* ICC8001
Forward primer†	CATGCCATGGGTCATGAGGCGGGGGAGT TTTTC
Reverse primer‡	CCGCTCGAGTTAGAACCGATAGCCTGCG GAGAA
Cloning vector	pTAMANHISTEV
Expression vector	pTAMANHISTEV
Expression host	*E. coli*
Complete amino-acid sequence of the construct produced§	MRYIRQLCCVSLLCLSGSAAAANVRLQH HHHHHHDYDIPTTENLYFQGAMGHEAG EFFIRAGTATVRPTEGSDNVLGSLGSF NVSNNTQLGLTFTYMATDNIGVELLAA TPFRHKVGTGPTGTIATVHQLPPTLMA QWYFGDAQSKVRPYVGAGINYTTFFNE DFNDTGKAAGLSDLSLKDSWGAAGQVG LDYLINRDWLLNMSVWYMDIDTDVKFK AGGVDQKVSTRLDPWVFMFSAGYRF

† The NcoI restriction site is underlined. ‡ The XhoI restriction site is underlined. § The pTAMA signal sequence that is not present after cleavage is underlined.

2.2. Crystallization

Purified $OmpW_{KP}$ underwent preliminary screening by the sitting-drop vapour-diffusion method at 293 K using the sparse-matrix MemGold screen (Molecular Dimensions). The protein was mixed with the precipitant in a 1:1 ratio using a Mosquito LCP crystallization robot (SPT Labtech).

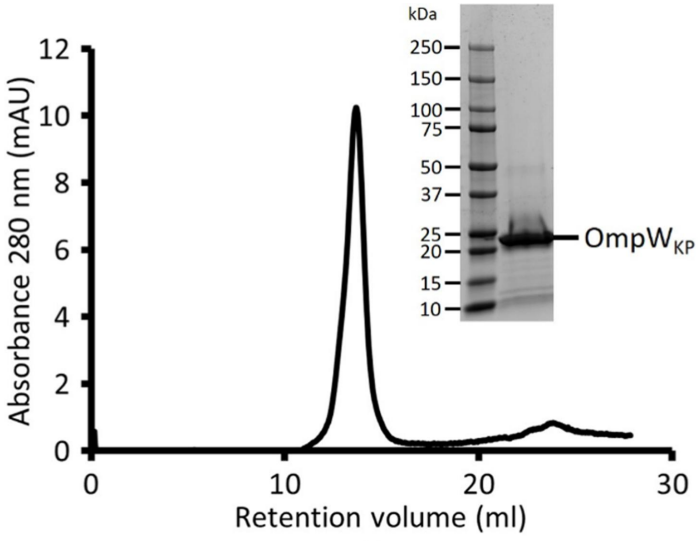

(*a*)

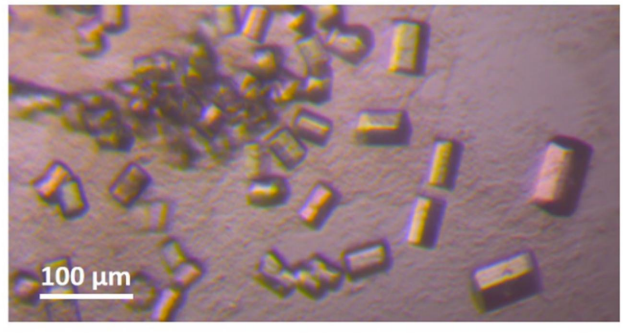

(*b*)

Figure 1
Purification and crystallization of $OmpW_{KP}$ (*a*) SEC analysis of $OmpW_{KP}$ shows a monodisperse peak, with SDS–PAGE analysis of purified $OmpW_{KP}$; the purity is greater than 95%. (*b*) Orthorhombic $OmpW_{KP}$ crystals. The largest crystals had dimensions of 100 × 20 × 20 µm.

Table 2
Data collection and processing.

Values in parentheses are for the outer shell.

Diffraction source	I03, DLS
Wavelength (Å)	0.9763
Temperature (K)	100
Detector	EIGER2 XE 16M
Space group	*C*222
a, *b*, *c* (Å)	87.92, 138.63, 52.96
α, β, γ (°)	90.0, 90.0, 90.0
Mosaicity (°)	0.15
Resolution range (Å)	52.9–3.2 (3.3–3.2)
Total No. of reflections	71778 (7496)
No. of unique reflections	5639 (560)
Completeness (%)	100 (100)
Multiplicity	12.7 (13.4)
$CC_{1/2}$	0.85 (0.99)
$\langle I/\sigma(I)\rangle$	64 (2.5)
$R_{r.i.m.}$	0.082 (0.207)
Overall *B* factor from Wilson plot (Å^2)	78.7

Table 3
Structure solution and refinement.

Values in parentheses are for the outer shell.

Resolution range (Å)	52.97–3.20 (3.31–3.20)
Completeness (%)	100 (100)
No. of reflections, working set	5633 (559)
No. of reflections, test set	236 (25)
Final R_{cryst}	0.2668 (0.2646)
Final R_{free}	0.3117 (0.3636)
No. of non-H atoms	
Protein	1388
Ion	10
Total	1398
R.m.s. deviations	
Bond lengths (Å)	0.003
Angles (°)	0.622
Average *B* factors (Å^2)	77.7
Protein	77.5
Ion	101.8
Ramachandran plot	
Most favoured (%)	95.98
Allowed (%)	3.45
Outliers (%)	0.57 [Pro113]

Orthorhombic crystals appeared after 24 h in the following condition: 0.35 *M* lithium sulfate, 0.1 *M* sodium acetate pH 4.0, 11% PEG 600. Large $OmpW_{KP}$ crystals were obtained by the hanging-drop vapour-diffusion method. Crystals were cryo-protected in a mixture of well solution supplemented with 30% PEG 600.

2.3. Data collection and processing

Diffraction data were collected on the I03 beamline at Diamond Light Source (DLS), Didcot, United Kingdom using an EIGER2 XE 16M detector. The crystals belonged to space group *C*222. Diffraction frames were indexed and integrated using the *DIALS* pipeline as implemented at DLS (Winter *et al.*, 2018). The data were scaled using *AIMLESS* in the *CCP*4 suite (Evans & Murshudov, 2013; Agirre *et al.*, 2023). The data-collection parameters and merging statistics are summarized in Table 2.

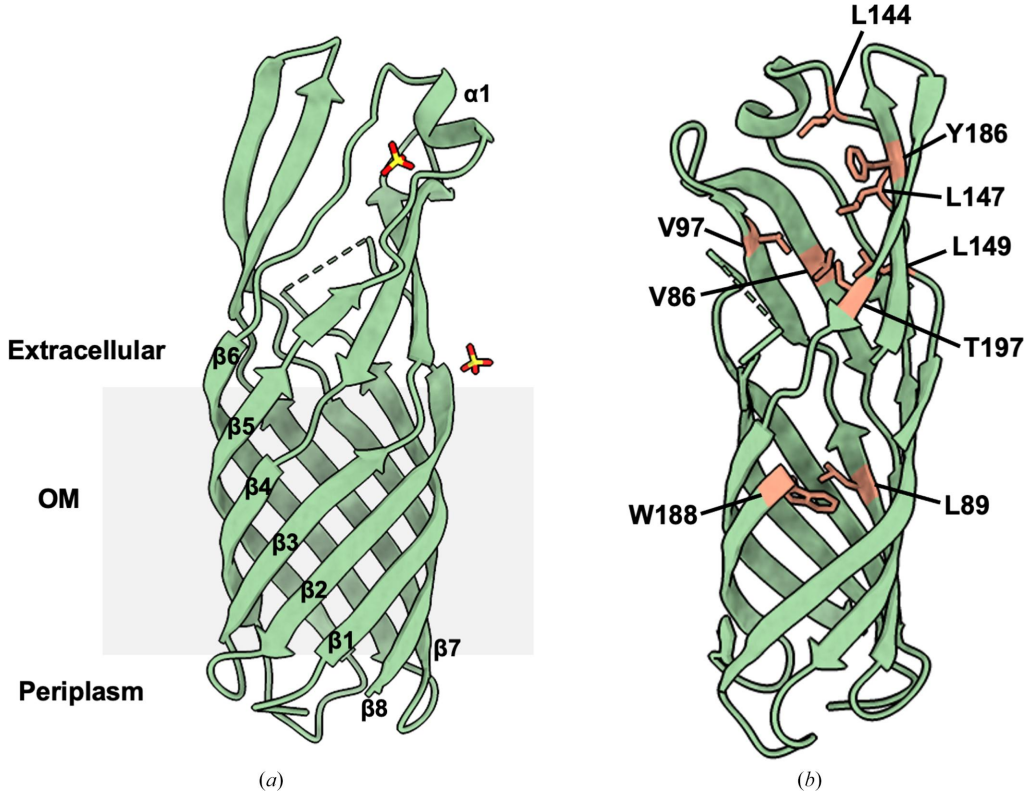

Figure 2
Structure of $OmpW_{KP}$. (*a*) Cartoon representation of the $OmpW_{KP}$ structure (shown in green) perpendicular to the OM (depicted in grey). Sulfate ions are depicted as sticks (O atoms are shown in red and S atoms in yellow). The missing residues are marked with a green dashed line. (*b*) The hydrophobic residues lining the extracellular region and forming the hydrophobic gate, Leu89 and Trp188, are shown as orange sticks.

2.4. Structure solution, model building and refinement

The structure of $OmpW_{KP}$ was solved by molecular replacement with the *AlphaFold*-predicted model of $OmpW_{KP}$ (Jumper *et al.*, 2021) using *Phenix* (Liebschner *et al.*, 2019). The calculated Matthews coefficient (V_M) was 3.84 Å^3 Da^{-1}, suggesting the presence of one molecule of $OmpW_{KP}$ in the asymmetric unit; this corresponds to a solvent content of 68% by volume. Manual adjustments to the model were performed in *Coot* (Emsley *et al.*, 2010). Density for two sulfate ions was present and they were included in the model. *Phenix* was used for refinement (Afonine *et al.*, 2018). *MolProbity* was used for validation (Williams *et al.*, 2018). Figure preparation was performed using *UCSF ChimeraX* 1.6 (Pettersen *et al.*, 2021). Refinement statistics are summarized in Table 3.

3. Results and discussion

3.1. Purification and crystallization of $OmpW_{KP}$

$OmpW_{KP}$ was overexpressed in *E. coli* and purified in C_8E_4 to homogeneity by immobilized metal affinity chromatography. $OmpW_{KP}$ displays a monodisperse peak on size-exclusion chromatography and was >95% pure as judged by SDS–PAGE (Fig. 1*a*). $OmpW_{KP}$ crystals grew overnight from

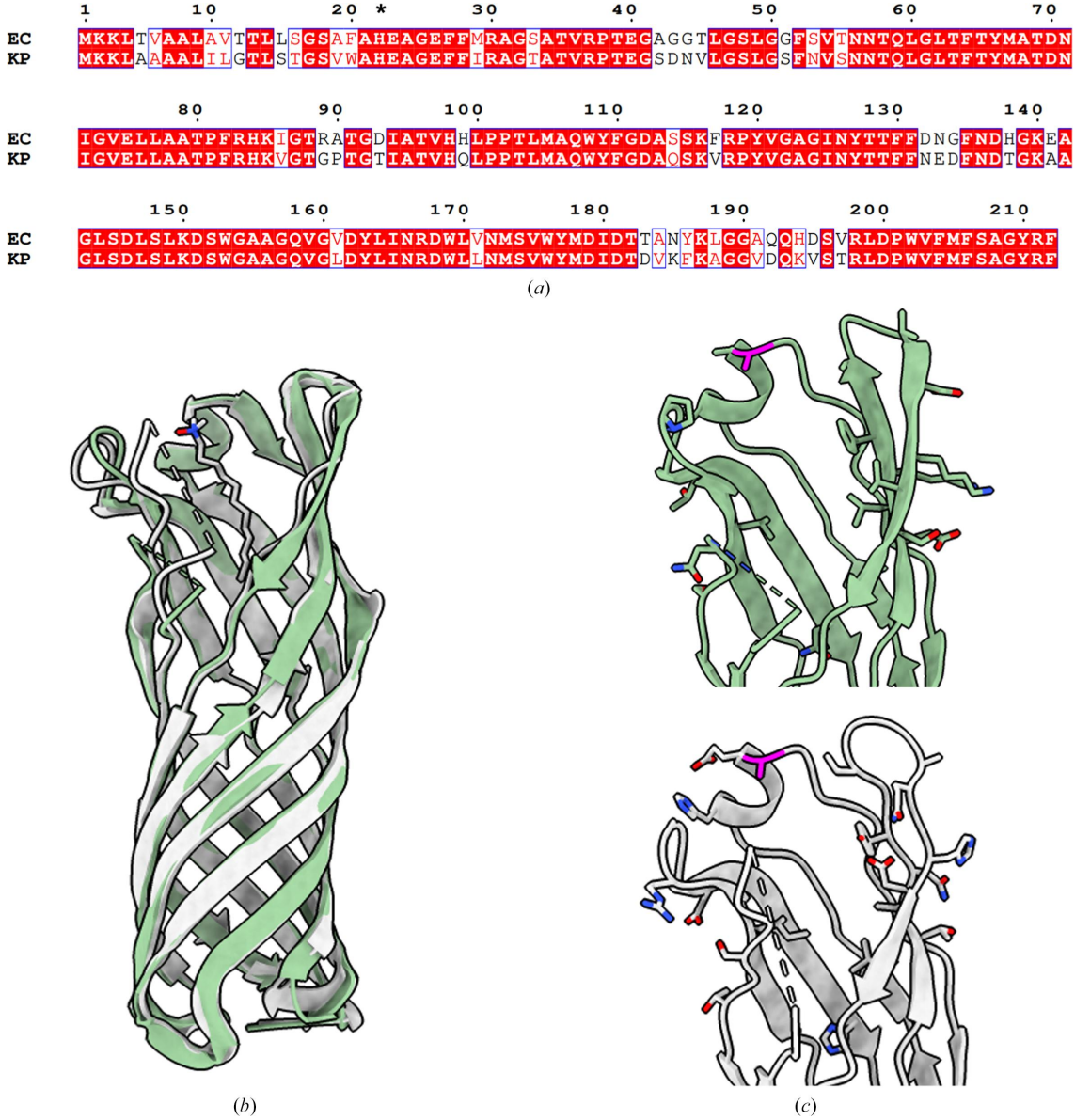

(*a*)

(*b*) (*c*)

Figure 3
Sequence alignment and superimposition of $OmpW_{KP}$ with $OmpW_{EC}$. (*a*) A sequence alignment of $OmpW_{EC}$ (UniProt ID P0A915) and $OmpW_{KP}$ (UniProt ID W9B759) is shown; conserved and similar residues are shown in red and blue boxes, respectively. Residue numbers are indicated above the protein sequences. An asterisk indicates the mature protein after cleavage of the signal peptide. The alignment was prepared using *ESPript* (Robert & Gouet, 2014). (*b*) $OmpW_{KP}$ (green) superimposed with $OmpW_{EC}$ (grey; PDB entry 2f1v; Hong *et al.*, 2006) shows high structural conservation. The LDAO molecule bound to $OmpW_{EC}$ is shown as sticks. (*c*) Close-up view of the extracellular regions of $OmpW_{KP}$ (green) and $OmpW_{EC}$ (grey), with the side chains of amino-acid differences shown as stick models. The conserved Ala142 is shown in magenta.

a solution consisting of 0.35 *M* lithium sulfate, 0.1 *M* sodium acetate pH 4.0, 11%(*w*/*v*) PEG 600 (Fig. 1*b*). The crystals had an orthorhombic shape and were further optimized by the hanging-drop vapour-diffusion method. The optimized crystals diffracted X-rays to 3.2 Å resolution and belonged to space group *C*222.

3.2. Structure solution of $OmpW_{KP}$

The structure of $OmpW_{KP}$ was solved by molecular replacement using the *AlphaFold*-predicted model. Continuous electron density could be observed for most of the structure except for Gly41–Phe52, which were omitted from model building. The $OmpW_{KP}$ structure consists of eight antiparallel β-strands (β1–β8) that arrange to form a hollow β-barrel in the OM and an extracellular solvent-exposed region (Fig. 2*a*). The extracellular region is formed from the extended β-strands of the barrel and a single α-helical turn (α1) connecting β5 and β6. A hydrophobic gate is present midway through the channel consisting of residues Leu89 and Trp188, as in $OmpW_{EC}$ (Hong *et al.*, 2006), where the extracellular entrance to the channel is lined with hydrophobic residues (Fig. 2*b*).

3.3. Comparison of $OmpW_{KP}$ with $OmpW_{EC}$

The closest structural homologue to $OmpW_{KP}$ is $OmpW_{EC}$, which shares 82.7% sequence identity and 88% sequence similarity (Fig. 3*a*). The two structures can be superimposed with an r.m.s.d. of 0.54 Å over 171 C^{α} atoms (Fig. 3*b*); they show high structural conservation of the β-barrel, with minor differences confined to the extracellular region, which displays some flexibility. The extracellular loop 1 that connects β1 and β2 is missing in both the $OmpW_{KP}$ and the $OmpW_{EC}$ structures, suggesting a highly flexible structure. This flexibility could be associated with substrate recruitment, as the conformation of the modelled loop 1 blocks the channel in the *AlphaFold*-predicted structure. In the $OmpW_{EC}$ structure an LDAO molecule is bound at the extracellular region but loop 1 is not fully resolved, suggesting that the inherited flexibility cannot be stabilized upon its binding (Hong *et al.*, 2006). This highly mobile structural element on the extracellular loop is likely to shield the hydrophobic face of the extracellular region and it could transiently open to recruit hydrophobic substrates. Despite the sequence conservation of loop 1 being low between $OmpW_{KP}$ and $OmpW_{EC}$, this suggests that it might be involved in substrate selectivity between different bacterial species.

Despite amino-acid differences in the extracellular region between $OmpW_{KP}$ and $OmpW_{EC}$ (Fig. 3*c*), where the tip of $TraN_{R100\text{-}1}$ has been shown to bind (Low *et al.*, 2023), binding of $TraN_{R100\text{-}1}$ is not impaired between the two species. We previously reported that Ala142, which is conserved between $OmpW_{KP}$ and $OmpW_{EC}$, acts as the minimum residue for specificity towards $TraN_{R100\text{-}1}$ (Low *et al.*, 2023); the equivalent residue in *Citrobacter rodentium* OmpW ($OmpW_{CR}$) is Asn142, which prevents R100-1 conjugation because of a steric clash with the tip of $TraN_{R100\text{-}1}$ (Low *et al.*, 2023). The N142A mutation in $OmpW_{CR}$ restored conjugation efficiency (Low *et al.*, 2023).

In conclusion, we have resolved the crystal structure of $OmpW_{KP}$; structural comparison with $OmpW_{EC}$ identified the presence of a highly flexible loop, loop 1, that might be important for shielding the pore prior to hydrophobic substrate recruitment. In addition, despite sequence and structural differences in the extracellular region, both porins can mediate interactions with TraNα.

Acknowledgements

We would like to thank Diamond Light Source for beam time on I03.

Funding information

This work was carried out with the funding of a BBSRC DTP Studentship grant (BB/M011178/1).

References

Afonine, P. V., Poon, B. K., Read, R. J., Sobolev, O. V., Terwilliger, T. C., Urzhumtsev, A. & Adams, P. D. (2018). *Acta Cryst.* D**74**, 531–544.

Agirre, J., Atanasova, M., Bagdonas, H., Ballard, C. B., Baslé, A., Beilsten-Edmands, J., Borges, R. J., Brown, D. G., Burgos-Mármol, J. J., Berrisford, J. M., Bond, P. S., Caballero, I., Catapano, L., Chojnowski, G., Cook, A. G., Cowtan, K. D., Croll, T. I., Debreczeni, J. É., Devenish, N. E., Dodson, E. J., Drevon, T. R., Emsley, P., Evans, G., Evans, P. R., Fando, M., Foadi, J., Fuentes-Montero, L., Garman, E. F., Gerstel, M., Gildea, R. J., Hatti, K., Hekkelman, M. L., Heuser, P., Hoh, S. W., Hough, M. A., Jenkins, H. T., Jiménez, E., Joosten, R. P., Keegan, R. M., Keep, N., Krissinel, E. B., Kolenko, P., Kovalevskiy, O., Lamzin, V. S., Lawson, D. M., Lebedev, A. A., Leslie, A. G. W., Lohkamp, B., Long, F., Malý, M., McCoy, A. J., McNicholas, S. J., Medina, A., Millán, C., Murray, J. W., Murshudov, G. N., Nicholls, R. A., Noble, M. E. M., Oeffner, R., Pannu, N. S., Parkhurst, J. M., Pearce, N., Pereira, J., Perrakis, A., Powell, H. R., Read, R. J., Rigden, D. J., Rochira, W., Sammito, M., Sánchez Rodríguez, F., Sheldrick, G. M., Shelley, K. L., Simkovic, F., Simpkin, A. J., Skubak, P., Sobolev, E., Steiner, R. A., Stevenson, K., Tews, I., Thomas, J. M. H., Thorn, A., Valls, J. T., Uski, V., Usón, I., Vagin, A., Velankar, S., Vollmar, M., Walden, H., Waterman, D., Wilson, K. S., Winn, M. D., Winter, G., Wojdyr, M. & Yamashita, K. (2023). *Acta Cryst.* D**79**, 449–461.

Beis, K., Whitfield, C., Booth, I. & Naismith, J. H. (2006). *Int. J. Biol. Macromol.* **39**, 10–14.

Emsley, P., Lohkamp, B., Scott, W. G. & Cowtan, K. (2010). *Acta Cryst.* D**66**, 486–501.

Evans, P. R. & Murshudov, G. N. (2013). *Acta Cryst.* D**69**, 1204–1214.

Frankel, G., David, S., Low, W. W., Seddon, C., Wong, J. C. & Beis, K. (2023). *Nucleic Acids Res.* **51**, 8925–8933.

Hong, H., Patel, D. R., Tamm, L. K. & van den Berg, B. (2006). *J. Biol. Chem.* **281**, 7568–7577.

Huang, W., Wang, S., Yao, Y., Xia, Y., Yang, X., Long, Q., Sun, W., Liu, C., Li, Y. & Ma, Y. (2015). *Vaccine*, **33**, 4479–4485.

Jumper, J., Evans, R., Pritzel, A., Green, T., Figurnov, M., Ronneberger, O., Tunyasuvunakool, K., Bates, R., Žídek, A., Potapenko, A., Bridgland, A., Meyer, C., Kohl, S. A. A., Ballard, A. J., Cowie, A., Romera-Paredes, B., Nikolov, S., Jain, R., Adler, J., Back, T., Petersen, S., Reiman, D., Clancy, E., Zielinski, M., Steinegger, M., Pacholska, M., Berghammer, T., Bodenstein, S., Silver, D., Vinyals, O., Senior, A. W., Kavukcuoglu, K., Kohli, P. & Hassabis, D. (2021). *Nature*, **596**, 583–589.

Lederberg, J. & Tatum, E. L. (1946). *Nature*, **158**, 558.
Liebschner, D., Afonine, P. V., Baker, M. L., Bunkóczi, G., Chen, V. B., Croll, T. I., Hintze, B., Hung, L.-W., Jain, S., McCoy, A. J., Moriarty, N. W., Oeffner, R. D., Poon, B. K., Prisant, M. G., Read, R. J., Richardson, J. S., Richardson, D. C., Sammito, M. D., Sobolev, O. V., Stockwell, D. H., Terwilliger, T. C., Urzhumtsev, A. G., Videau, L. L., Williams, C. J. & Adams, P. D. (2019). *Acta Cryst.* D**75**, 861–877.
Lou, H., Beis, K. & Naismith, J. H. (2009). *Curr. Top. Membr.* **63**, 269–297.
Low, W. W., Seddon, C., Beis, K. & Frankel, G. (2023). *J. Bacteriol.* **205**, e00061-23.
Low, W. W., Wong, J. L. C., Beltran, L. C., Seddon, C., David, S., Kwong, H., Bizeau, T., Wang, F., Peña, A., Costa, T. R. D., Pham, B., Chen, M., Egelman, E. H., Beis, K. & Frankel, G. (2022). *Nat. Microbiol.* **7**, 1016–1027.
Miroux, B. & Walker, J. E. (1996). *J. Mol. Biol.* **260**, 289–298.
Pagès, J., James, C. E. & Winterhalter, M. (2008). *Nat. Rev. Microbiol.* **6**, 893–903.
Pettersen, E. F., Goddard, T. D., Huang, C. C., Meng, E. C., Couch, G. S., Croll, T. I., Morris, J. H. & Ferrin, T. E. (2021). *Protein Sci.* **30**, 70–82.
Robert, X. & Gouet, P. (2014). *Nucleic Acids Res.* **42**, W320–W324.
Williams, C. J., Headd, J. J., Moriarty, N. W., Prisant, M. G., Videau, L. L., Deis, L. N., Verma, V., Keedy, D. A., Hintze, B. J., Chen, V. B., Jain, S., Lewis, S. M., Arendall, W. B. III, Snoeyink, J., Adams, P. D., Lovell, S. C., Richardson, J. S. & Richardson, D. C. (2018). *Protein Sci.* **27**, 293–315.
Winter, G., Waterman, D. G., Parkhurst, J. M., Brewster, A. S., Gildea, R. J., Gerstel, M., Fuentes-Montero, L., Vollmar, M., Michels-Clark, T., Young, I. D., Sauter, N. K. & Evans, G. (2018). *Acta Cryst.* D**74**, 85–97.
Wu, X., Tian, L., Zou, H., Wang, C., Yu, Z., Tang, C., Zhao, F. & Pan, J. (2013). *Res. Microbiol.* **164**, 848–855.